

Ground-state properties and structure evolutions of odd- A transuranium Bk isotopes by deformed relativistic Hartree-Bogoliubov theory in continuum

Zi-Dan Huang,¹ Wei Zhang,¹ Shuang-Quan Zhang,² and Ting-Ting Sun^{1,*}

¹*School of Physics, Zhengzhou University, Zhengzhou 450001, China*

²*State Key Laboratory of Nuclear Physics and Technology,
School of Physics, Peking University, Beijing 100871, China*

The studies of transuranium nuclei are of vital significance in exploring the existence of the “island of superheavy nuclei”. This work presents the systematic investigations for the ground-state properties and structure evolutions of odd- A transuranium Bk isotopes taking the deformed relativistic Hartree-Bogoliubov theory in continuum (DRHBc) with PC-PK1 density functional, in comparison with those by spherical relativistic continuum Hartree-Bogoliubov (RCHB) theory. The DRHBc calculations offer improved descriptions of the binding energies, closely aligning with the experimental data. The incorporation of deformation effects in DRHBc results in enhanced nuclear binding energies and a notable reduction in α -decay energies. With the rotational corrections further incorporated, the theoretical deviation by DRHBc from the experimental data is further reduced. Based on the two-neutron gap δ_{2n} and the neutron pairing energy E_{pair}^n , prominent shell closures at $N = 184$ and 258 , as well as potential sub-shell structures at $N = 142, 150, 162, 178, 218,$ and 230 are exhibited. A quasi-periodic variation among prolate, oblate, and spherical shapes as well as prolate deformation predominance have been shown in the evolutions of the quadrupole deformation. Possible shape coexistence is predicted in ^{331}Bk with the oblate and prolate minima in close energies, which is further supported by the triaxial relativistic Hartree-Bogoliubov theory in continuum (TRHBc) calculations.

I. INTRODUCTION

Element $Z = 92$, uranium (U), is the heaviest element that naturally exists on Earth [1]. So far, 26 transuranium elements have been synthesized artificially, ranging from $Z = 93$ to $Z = 118$ [1–3], and the 7th period of the periodic table of elements has been completed. Meanwhile, many theoretical studies predicted the existence of the “island of superheavy nuclei” near $Z = 114$ and $N = 184$ [4–10]. Thereafter, exploring the island of superheavy nuclei has become as one of the foremost scientific objectives in both experimental research at large-scale facilities and theoretical investigations [11–14]. Extensive investigations on the nuclear structure, decay modes, and reactions have been performed for superheavy nuclei [15–20]. Among these aspects, the shell structure and magic numbers, the position of the island of superheavy nuclei, as well as the ground state properties such as mass and shape are some key issues for structures of superheavy nuclei which have been achieving great attentions [11].

A variety of theoretical models have been developed or employed to investigate the structures and properties of transuranium isotopes and superheavy nuclei [16, 21], including several empirical formulas such as the ab formula [22], macroscopic-microscopic models [23, 24], configuration-constrained total-Routhian-surface method [25, 26], self-consistent mean-field models [24, 27, 28], quasiparticle phonon model [29], particle-rotor model [30], projected shell model [31–33], multi-

shell shell model for heavy nuclei [34], cranking shell model [35–37], etc.

The quantum shell effect is the fundamental reason for the existence of superheavy nuclei. Early nuclear structure theories predicted that the atomic nucleus with $Z = 114$ and $N = 184$ was doubly magic after ^{208}Pb . Recent macroscopic-microscopic models still give the same prediction [38]. However, microscopic models give different predictions. For example, in Ref. [39], taking the Skyrme-Hartree-Fock model, Rutz *et al.* predicted magic numbers $Z = 120$ and $N = 172$, $Z = 126$ and $N = 184$ besides $Z = 114$ and $N = 184$. In Ref. [40], taking the spherical relativistic continuum Hartree-Bogoliubov (RCHB) theory, Zhang *et al.* predicted the proton magic numbers $Z = 120, 132, 138$ and neutron magic numbers $N = 172, 184, 198, 228, 238, 258$ by examining various physical quantities, such as two-neutron/proton separation energies, two-neutron/proton gaps, shell correction energy, pairing energy, and pairing gap. By further including the deformation, tensor force, and Fock term, different shell structures have been predicted in superheavy nuclei [41, 42]. For example, in Ref. [42], taking the spherical relativistic continuum Hartree-Fock-Bogoliubov model, Li *et al.* predicted proton magic numbers $Z = 120, 138$ and neutron magic numbers $N = 172, 184, 228, 258$. In Ref. [43], taking macroscopic-microscopic models, Patyk and Sobiczewski studied the effects of high-order deformation on nuclear shell structures and revealed ^{270}Hs being a deformed double magic nucleus. They also pointed out that relatively stable deformed superheavy nuclei exist in the region of $Z = 108$ and $N = 162$, which has been further confirmed by Pei *et al.* through the studies taking the Skyrme-Hartree-Fock+BCS model [44]. Besides the important role of

*Corresponding author, ttsunphy@zzu.edu.cn

nuclear deformation on the shell structures, many studies have proved its significance, such as for single-particle structures [45, 46], deformed halos [47–51], fission barriers [52–54], shape coexistence [55–57], α decay [58] and electron capture cross section [59].

The deformed relativistic Hartree-Bogoliubov theory in continuum (DRHBc) theory [47, 60, 61], which can concurrently take into account pairing correlations, continuum effects, and degrees of freedom in deformation, is one of the most potent models. Based on the DRHBc theory, numerous interesting studies have been conducted, such as the prediction of shape-decoupling between the core and halo in deformed halo nuclei [47, 62–65], the resolution of the puzzles regarding the radius and neutron configuration in ^{22}C [66], the number of particles in the classically forbidden regions for magnesium isotopes [67], the deformation effects on the neutron drip line [68], the shape evolution, shape coexistence and prolate-shape dominance [69–72], the fission barrier [52], the evolution of shell closures [73, 74], the stability peninsulas beyond the neutron drip line [18, 75–77], the one-proton emission from $^{148-151}\text{Lu}$ [78, 79], the dependence on the multipole expansion order [80], the optimization of Dirac-Woods-Saxon (DWS) basis [81], the rotational excitations of exotic nuclei with angular momentum projection [63, 82], and the dynamical correlation with a two-dimensional collective Hamiltonian method [83].

With a proton number of $Z = 97$, Bk is located almost in the middle between the proton shell of $Z = 82$ and the possible proton shells $Z = 114, 120, 126$. From an experimental perspective, it is proposed that ^{249}Bk is an ideal target for synthesizing elements 119 and 120 [84]. However, a systematic and detailed research on the properties of Bk isotopes is still absent and urgently desired. In this paper, we will systematically investigate the ground-state properties and structure evolutions of odd- A transuranium Bk isotopes. Matters such as the determination of drip lines, shell structures and magic numbers, the impact of deformation on binding energies and radii, shape evolution and shape coexistence will be inspected. This paper is organized as follows: the DRHBc theory will be succinctly introduced in Section II, after presenting the results and discussions in Section III, finally a summary will be offered in Section IV.

II. THEORETICAL FRAMEWORK AND NUMERICAL DETAILS

Detailed descriptions of the DRHBc theory can be found in Refs. [47, 61, 85]. Here, we briefly introduce the formalism for the convenience of discussions. In the DRHBc theory, the relativistic Hartree-Bogoliubov (RHB) equation reads,

$$\begin{pmatrix} \hat{h}_D - \lambda_\tau & \hat{\Delta} \\ -\hat{\Delta}^* & -\hat{h}_D^* + \lambda_\tau \end{pmatrix} \begin{pmatrix} U_k \\ V_k \end{pmatrix} = E_k \begin{pmatrix} U_k \\ V_k \end{pmatrix}, \quad (1)$$

where \hat{h}_D represents the Dirac Hamiltonian, $\hat{\Delta}$ is the pairing potential, λ_τ is the Fermi energy for neutrons or protons ($\tau = n, p$), E_k is the quasiparticle energy, and U_k and V_k are the quasiparticle wave functions.

The Dirac Hamiltonian in the coordinate space is given by

$$h_D(\mathbf{r}) = \boldsymbol{\alpha} \cdot \mathbf{p} + V(\mathbf{r}) + \beta[M + S(\mathbf{r})], \quad (2)$$

where M is the nucleon mass, and $S(\mathbf{r})$ and $V(\mathbf{r})$ are the scalar and vector potentials, respectively. The pairing potential is expressed as,

$$\Delta(\mathbf{r}_1, \mathbf{r}_2) = V^{PP}(\mathbf{r}_1, \mathbf{r}_2) \kappa(\mathbf{r}_1, \mathbf{r}_2), \quad (3)$$

where $\kappa = V^*U^T$ is the pairing tensor and V^{PP} is the pairing force of a density-dependent zero-range type,

$$V^{PP}(\mathbf{r}_1, \mathbf{r}_2) = V_0 \frac{1}{2} (1 - P^\sigma) \delta(\mathbf{r}_1 - \mathbf{r}_2) \left(1 - \frac{\rho(\mathbf{r}_1)}{\rho_{\text{sat}}} \right), \quad (4)$$

with V_0 being the pairing strength, $\frac{1}{2}(1 - P^\sigma)$ the projector for the spin $S = 0$ component, and ρ_{sat} the saturation density of nuclear matter.

For an axially deformed nucleus with spatial reflection symmetry, the third component m of the angular momentum j and the parity π are conserved quantum numbers. Thus, the RHB Hamiltonian can be decomposed into blocks m^π characterized by m and parity π . Additionally, the potentials and densities in the DRHBc theory can be expanded in terms of Legendre polynomials [86],

$$f(\mathbf{r}) = \sum_{\lambda} f_{\lambda}(r) P_{\lambda}(\cos \theta), \quad \lambda = 0, 2, 4, \dots, \quad (5)$$

with

$$f_{\lambda}(r) = \frac{2\lambda + 1}{4\pi} \int d\Omega f(\mathbf{r}) P_{\lambda}(\cos \theta). \quad (6)$$

For an odd- A or odd-odd nucleus, one needs to further take into consideration the blocking effect for the unpaired single proton or neutron [66, 68, 87]. The equal filling approximation is adopted to deal with the blocking effects in the DRHBc theory [88].

The RHB equations are solved in the DWS basis [60, 72, 89, 90], which can appropriately describe the large spatial extension of weakly bound nuclei. In the numerical calculation, the angular momentum cutoff for the DWS basis is chosen as $J_{\text{max}} = \frac{23}{2}h$. The maximum expansion order in Eq. (5) is $\lambda_{\text{max}} = 8$, which is sufficient for our study [88, 91]. The size of the box is set to be 20 fm, and the energy cutoff in the Fermi sea is $E_{\text{cut}}^+ = 300$ MeV. For the particle-particle channel, we use the zero-range pairing force with a saturation density $\rho_{\text{sat}} = 0.152 \text{ fm}^{-3}$ and a pairing strength $V_0 = -325 \text{ MeV} \cdot \text{fm}^3$ [68, 92]. All the numerical details are the same as those employed in constructing the DRHBc mass tables [92, 93].

III. RESULTS AND DISCUSSION

In this section, to reveal the ground-state properties and the structure evolutions of the odd- A transuranium Bk isotopes, systematic calculations, such as those for the binding energy, two-neutron and two-proton separation energies, α decay energy, Fermi energy, two-neutron gap, pairing energy, and potential energy curves have been carried out from the proton drip line to the neutron drip line based on the DRHBc theory. The results are further compared with the available experimental data [94] and those from the spherical RCHB calculations [95].

In Fig. 1(a), the binding energies per nucleon E_b/A for the odd- A Bk isotopes are depicted as a function of the neutron number N and compared with the RCHB results and the available data. Within the range of available experimental data, the calculation outcomes by DRHBc are in good accordance with the experimental data, whereas the results by RCHB deviate significantly from the experimental results. This implies that deformation effects have a considerable influence on the binding energies of those nuclei. The nucleus ^{239}Bk has the largest specific binding energy experimentally, which is reproduced by the DRHBc calculations. When comparing with the RCHB results, the DRHBc gives very similar specific binding energies near the possible neutron shell closures, namely $N = 184$ and $N = 258$, while visible differences are exhibited when deviating the magic neutron numbers, especially at the mid-shell regions.

Fig. 1(b) presents the two-neutron separation energies $S_{2n}(Z, N) = E_b(Z, N) - E_b(Z, N - 2)$ as a function of the neutron number N by both DRHBc and RCHB theories, in comparison with the experimental data [94]. For both DRHBc and RCHB calculations, S_{2n} gradually decreases with the increasing neutron number, drops sharply at $N = 184$, then remains about 3 MeV within a large mass range until it drops sharply again at $N = 258$, and finally becomes negative at $N = 260$, indicating that ^{355}Bk is the neutron drip-line nucleus for the Bk isotopes. This evolution also demonstrates that $N = 184$ and 258 are two magic numbers for neutrons. Compared to the RCHB calculations, DRHBc reproduces the available experimental data much better. Furthermore, remarkable crossings of S_{2n} within two shell closures can be found between the results by DRHBc and RCHB. For instance, from $N = 184$ to 258, the S_{2n} values by DRHBc are larger than those by RCHB for nuclei before mid-shell, and the opposite holds true after that. The main reason can be attributed to the deformation effect encompassed in DRHBc calculations. The difference of S_{2n} between the DRHBc and RCHB can be delineated as follows,

$$\begin{aligned} \Delta S_{2n}(Z, N) &= S_{2n}(\text{DRHBc}) - S_{2n}(\text{RCHB}) \\ &= \Delta E_b(Z, N) - \Delta E_b(Z, N - 2) \\ &= 2 \frac{\partial \Delta E_b}{\partial N} \propto \frac{\partial \Delta |\beta_2|}{\partial N} \equiv \frac{\partial |\beta_2|}{\partial N}, \quad (7) \end{aligned}$$

where ΔE_b and $\Delta |\beta_2|$ denote the difference between the DRHBc and RCHB results for E_b and $|\beta_2|$, respectively.

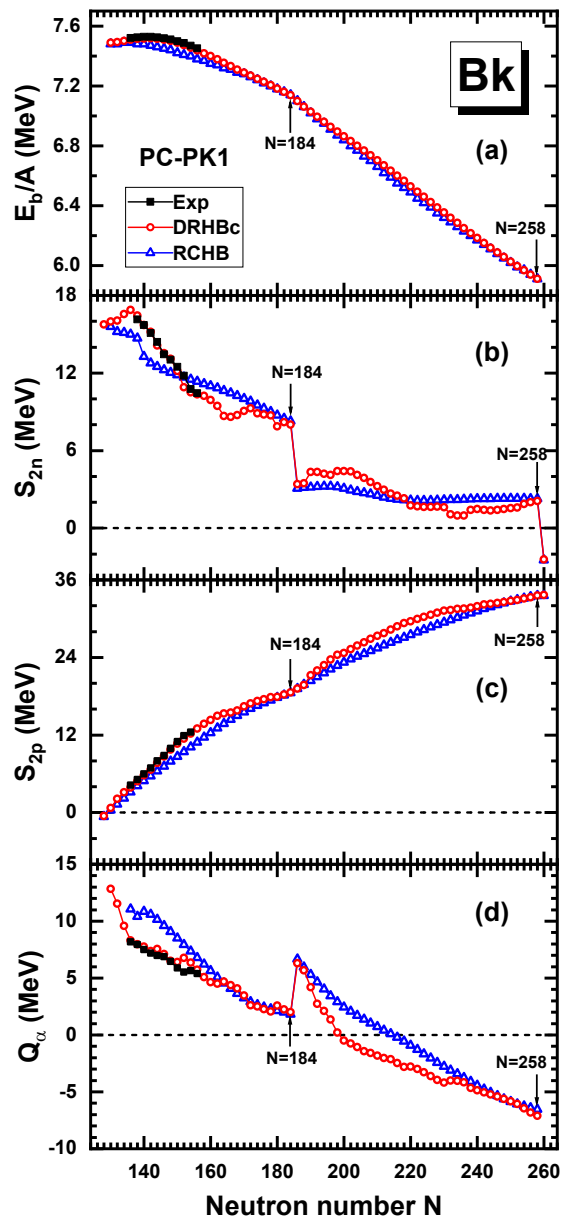


Figure 1: (Color online) (a) Binding energy per nucleon E_b/A , (b) two-neutron separation energy S_{2n} , (c) two-proton separation energy S_{2p} , and (d) α decay energy Q_α as functions of the neutron number for the odd- A Bk isotopes obtained in the DRHBc calculations with PC-PK1. The results by the RCHB calculations [95] and the available experimental data [94] are presented for comparison.

Due to the spherical assumption in RCHB, $\Delta |\beta_2|$ is always equal to $|\beta_2|$ obtained by DRHBc. The symbol \propto represents that the ΔE_b strongly correlates with $\Delta |\beta_2|$, i.e., the gain in binding energy due to deformation, expressed by the energy difference ΔE_b , is consistent with the absolute value of the deformation parameter as discussed in Ref. [68]. In general, as the nucleon number moves away from the shell closure to the mid-shell, deformed structures are developed while suppressed when

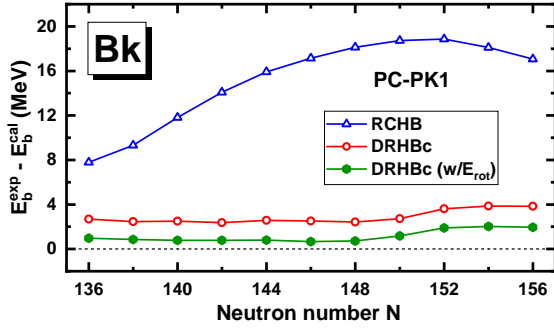


Figure 2: (Color online) The difference of the total binding energy $E_b^{\text{exp}} - E_b^{\text{cal}}$ between the experimental data and the DRHBc results with and without the rotation correction E_{rot} . The RCHB results [95] are also provided for comparison.

nucleon number increases from the mid-shell to the next shell closure. According to this kind of deformation evolution within two shell closures, $\frac{\partial|\beta_2|}{\partial N} > 0$ before mid-shell, $\frac{\partial|\beta_2|}{\partial N} < 0$ after mid-shell and $\frac{\partial|\beta_2|}{\partial N} = 0$ around mid-shell. Consequently, S_{2n} in DRHBc are greater than those in RCHB for nuclei before mid-shell while smaller after mid-shell. Around the mid-shell, the S_{2n} values in DRHBc and RCHB are close to each other which then results in the crossings of S_{2n} in Fig. 1(b). In addition, as discussed in Ref. [68], the inclusion of deformation may extend or shrink the position of drip line depending on the evolution of the degree of deformation. For Bk isotopic chain, due to spherical shapes for nuclei around the drip line, the identical positions of the drip line are predicted by DRHBc and RCHB.

Fig. 1(c) presents the two-proton separation energies $S_{2p}(Z, N) = E_b(Z, N) - E_b(Z - 2, N)$ as a function of the neutron number N . The S_{2p} increases with the increasing neutron number and presents kink structures at the shell closures of $N = 184$ and 258 . Similar to S_{2n} , the difference of S_{2p} between the DRHBc and RCHB calculations reads,

$$\begin{aligned} \Delta S_{2p}(Z, N) &= S_{2p}(\text{DRHBc}) - S_{2p}(\text{RCHB}) \\ &= \Delta E_b(Z, N) - \Delta E_b(Z - 2, N) \\ &\approx 2 \frac{\partial \Delta E_b}{\partial Z} : \propto \frac{\partial \Delta |\beta_2|}{\partial Z} \equiv \frac{\partial |\beta_2|}{\partial Z}, \end{aligned} \quad (8)$$

which means the sign of $\Delta S_{2p}(Z, N)$ is determined by $\frac{\partial |\beta_2|}{\partial Z}$. Since the Bk ($Z = 97$) isotopes are more deformed than the corresponding Am ($Z = 95$) isotones as seen in Ref. [96], the $\Delta S_{2p}(Z, N)$ will be positive. As a result, compared with the RCHB results, the DRHBc predicts larger S_{2p} for Bk isotopes as shown in Fig. 1(c). In addition, on the neutron-deficient side, S_{2p} changes from positive to negative from $N = 130$ to 128 by both the DRHBc and RCHB theories, indicating the same proton drip-line nucleus ^{227}Bk .

Fig. 1(d) presents the α -decay energies $Q_\alpha(Z, N) = E_b(Z - 2, N - 2) + E_b(2, 2) - E_b(Z, N)$ as a function of

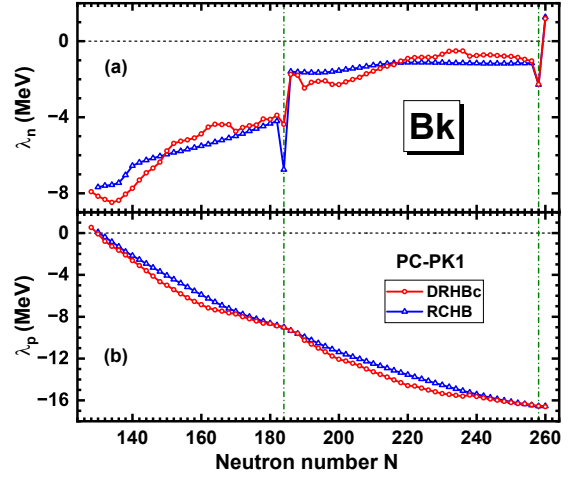


Figure 3: (Color online) The (a) neutron and (b) proton Fermi energies of the Bk isotopes obtained by the DRHBc calculations as functions of the neutron number. The RCHB results in Ref. [95] are also presented for comparison.

the neutron number N . With the inclusion of deformation, the DRHBc results are in good consistency with the experimental data. In general, the Q_α decreases gradually with the neutron number N with a sudden increase at the shell closure of $N = 184$, and then becomes negative at $N = 200$. Compared with the RCHB results, Q_α values in DRHBc predications get significantly reduced for Bk isotopes before mid-shell. This behavior can be understood by the S_{2n} and S_{2p} shown in Figs. 1(b) and 1(c). In fact, Q_α can be written in a form of S_{2n} and S_{2p} as $Q_\alpha(Z, N) = E_b(2, 2) - S_{2p}(Z, N - 2) - S_{2n}(Z, N)$. The difference of Q_α between DRHBc and RCHB results is the consequence of the crossings of S_{2n} in Fig. 1(b) and the larger S_{2p} of the DRHBc in Fig. 1(c). It is noted that the last Bk isotope predicted to have α decay by the DRHBc theory ($N = 198$) has 16 fewer neutrons than that by RCHB ($N = 214$).

In Fig. 2, the difference of the total binding energy between the experimental data and the DRHBc results $E_b^{\text{exp}} - E_b^{\text{cal}}$ are plotted, in comparison with the RCHB results [95]. We further take the rotational correction E_{rot} (for the details, see Ref. [60, 61]) into account for the total binding energies E_b in the DRHBc calculations. As already discussed in Fig. 1(a), compared with the RCHB results [95], the DRHBc calculations have already prominently improved the predicted binding energies with the deformation effects being considered. With the rotational corrections further incorporated, the theoretical deviation from the experimental data is further reduced by almost 2 MeV to a root-mean-square error of 1.23 MeV. Hence, it can be concluded that the rotational corrections also have considerable impacts on the binding energies of Bk isotopes.

Within the mean-field framework, the Fermi energy represents the variation of the total energy with respect to the particle number and conveys information regard-

ing the drip line position. Fig. 3(a) presents the neutron Fermi energy λ_n as a function of the neutron number N by both the DRHBc and RCHB theories. In both DRHBc and RCHB calculations, λ_n rises continuously with neutron number and a remarkable increase happens at shell closure of $N = 184$. It surpasses the continuum threshold of 0 MeV at $N = 260$, indicating the neutron drip-line nucleus being ^{355}Bk , which is consistent with the prediction by the criterion of S_{2n} shown in Fig. 1(b). It is noted that λ_n for ^{281}Bk and ^{355}Bk are given by the last occupied single-proton level due to the pairing collapse. Crossings of λ_n within two shell closures can be found between the results by DRHBc and RCHB. For instance, from $N = 184$ to 258, the λ_n values by DRHBc are smaller than those by RCHB for nuclei before mid-shell while the opposite holds true after the mid-shell. This can be accounted for by the different single-particle (s.p.) level structures in the spherical and deformed cases. The s.p. levels with the same total angular momentum j are degenerate when spherical and will split into $(2j + 1)/2$ levels with the third component $\Omega = 1/2, 3/2, \dots, j/2$ when quadrupole deformed. The last occupied level in the deformed case is lower than that in the spherical case for nuclei before mid-shell while opposite after mid-shell.

Fig. 3(b) presents the proton Fermi energy λ_p for Bk isotopes as a function of neutron number N . With the increasing neutron number N , as the mean-field potential for protons will be deepen, the value of λ_p decreases correspondingly by both RCHB and DRHBc. Besides, kink structures are presented at the shell closures of $N = 184$ and 258. Compared with RCHB results, λ_p predicted by DRHBc are smaller generally. This can be explained by the different proton s.p. structures in the spherical and deformed cases, similar to the case of λ_n in Fig. 3(a). As the Bk isotopes with $Z = 97$ are positioned before the mid-shell between proton shell closures of $Z = 82$ and 126, the last occupied proton level in the deformed case is lower than that in the spherical case. In addition, on the neutron-deficient side, λ_p surpasses the continuum threshold of 0 MeV at $N = 128$, indicating ^{227}Bk as the proton drip-line nucleus in DRHBc, which is the same as that predicted according to S_{2p} in Fig. 1(c). The proton drip-line nucleus in the RCHB prediction is ^{229}Bk with two more neutrons.

Compared with the S_{2n} in Fig 1(b), the two-neutron gap $\delta_{2n}(Z, N) = S_{2n}(Z, N) - S_{2n}(Z, N + 2)$ is more sensitive to the shell effects and thus it is often employed to search for the shell closures [40]. Fig 4(a) presents δ_{2n} for Bk isotopes as a function of the neutron number N by DRHBc, in comparison with the RCHB results and the available data. In general, the DRHBc results agree better with the available data [94] compared with the RCHB results. At $N = 184$ and 258, the δ_{2n} exhibits very sharp peaks, indicating significant shell closures there. It is noted that, in the DRHBc predictions, many small peaks also emerge, respectively at $N = 142, 150, 162, 178, 218,$ and 230 , corresponding to

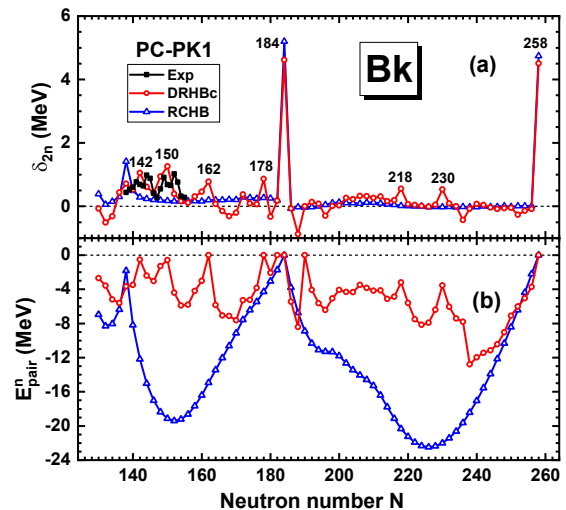


Figure 4: (Color online) (a) Two-neutron gap δ_{2n} and (b) neutron pairing energy E_{pair}^n as functions of the neutron number in the Bk isotopes obtained by the DRHBc calculations. The RCHB results [95] and the available experimental data [94] are also presented for comparison.

possible sub-shells. In contrast, only one additional peak appears at $N = 138$ in the RCHB predictions. Since the pairing energy can also reveal nuclear shell structures, in Fig. 4(b), we present the neutron pairing energies E_{pair}^n as a function of the neutron number N . In RCHB calculations, the E_{pair}^n shows very obvious large shell structures: the $|E_{\text{pair}}^n|$ approaches zero at shell closures of $N = 184$, and 258 or local minimum at $N = 138$ while maxima at mid-shells. In DRHBc calculations, many more peaks appear with the $|E_{\text{pair}}^n|$ approaching zero, respectively at $N = 142, 150, 162, 178, 182, 184, 190, 258$, or local minima at $N = 218, 230$, which are almost in one-to-one correspondence with the peaks of δ_{2n} . All those indicated by δ_{2n} and E_{pair}^n clearly signify the shell structures of Bk isotopes. However, the neutron shells predicted for Bk isotopes by DRHBc might differ from those in the superheavy nuclei with proton numbers $Z = 117 - 120$, where $N = 172$ is also predicted to be a large neutron shell, while the shell closure $N = 184$ vanishes in $Z = 119, 120$ [97].

In Fig. 5, the evolutions of the potential energy curves (PECs) by DRHBc are plotted for the Bk isotopes with $\Delta N = 8$ ranging from the proton drip line ^{227}Bk to the neutron drip line ^{355}Bk . Constrained calculations are done with a step of deformation $\Delta\beta_2 = 0.05$. For comparison, the ground-state deformations by unconstrained calculations are also plotted. For the proton drip-line nucleus ^{227}Bk , the PEC is very flat and a prolate ground state around $\beta_2 = 0.10$ is determined by both the constrained and unconstrained calculations. In a large mass range from ^{235}Bk to ^{259}Bk , distinct prolate global minima are predicted, which are much deeper than the local oblate minima. Instead, in ^{267}Bk , two minima in prolate and oblate sides have very close energies with the

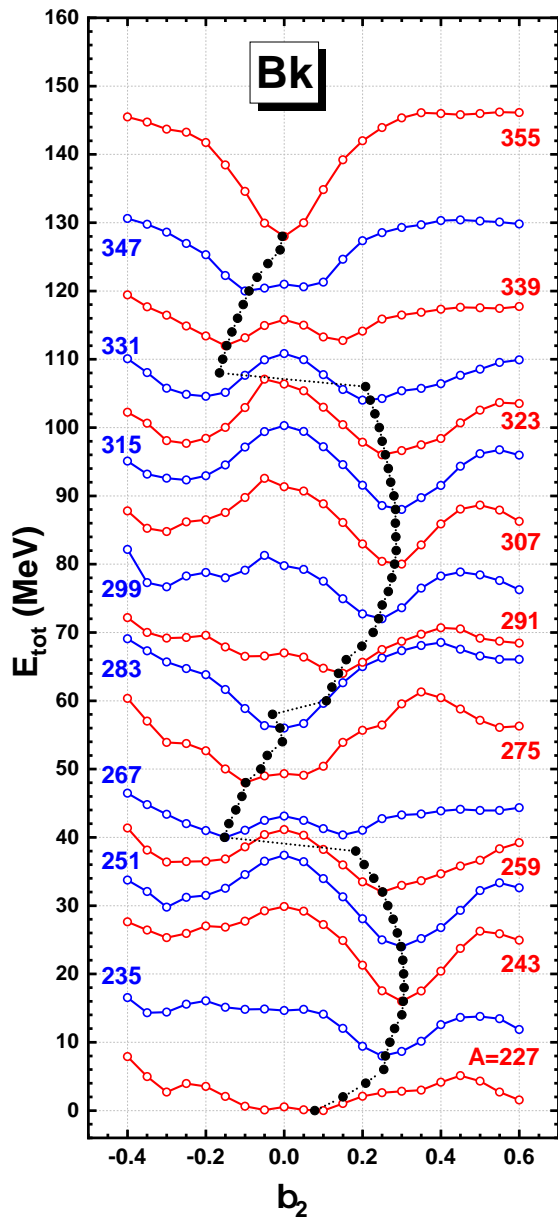


Figure 5: (Color online) Evolutions of the potential energy curves (PECs) denoted by open circles of $^{227,235,\dots,355}\text{Bk}$ isotopes with $\Delta N = 8$ obtained by the constrained DRHBc calculations with a step of deformation $\Delta\beta_2 = 0.05$. The PECs have been scaled to the energy of their ground states and shifted upward by 1 MeV for every one neutron. The ground-state deformations (solid circles) by unconstrained DRHBc calculations of odd- A Bk isotopes are also plotted.

difference as small as 0.35 MeV and a barrier height of 3.1 MeV between them, indicating the possible shape coexistence therein. The competition between the two energy minima ultimately determines the ground state in an oblate shape. The nuclear ground state remains oblate for several Bk isotopes until ^{283}Bk , which has only one energy minimum in spherical due to the neutron shell closure of $N = 184$. After the neutron number exceeds

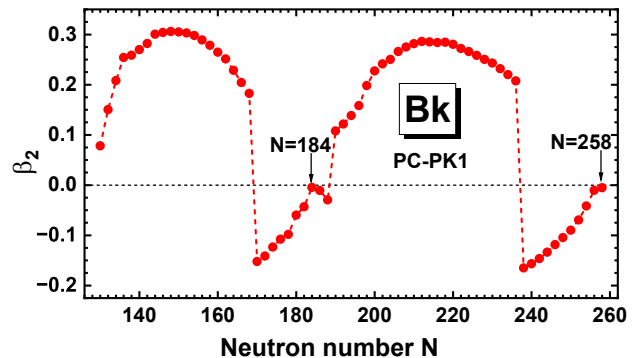


Figure 6: (Color online) Evolution of the quadrupole deformation β_2 for the Bk isotopes in ground states as functions of the neutron number N .

the magic number $N = 184$, the Bk isotopes again become prolate in a large mass range until ^{333}Bk . This prolate predominance [45] has also been observed in other isotopes [70, 98, 99]. As shown in Fig. 5, the PEC of ^{331}Bk has two energy minima with an energy difference of 0.57 MeV and a barrier of 6.8 MeV between them, presenting as another candidate for the possible shape coexistence. The ground state of ^{333}Bk is in prolate deformation while it turns to be oblate for ^{355}Bk . The oblate shape remains before the neutron number reaching the neutron shell closure of $N = 258$, where ^{355}Bk is spherical.

To show the shape evolution more intuitively, Fig. 6 presents the ground state deformation β_2 as a function of the neutron number N obtained by the unconstrained DRHBc calculations. From the proton drip line ^{227}Bk to the neutron drip line ^{355}Bk , the nuclear shape undergoes prolate, oblate, and spherical transitions between two shell closures, which is similar as depicted in the uranium isotopes [52]. In general, the shape is spherical at $N = 184, 258$, while deformed when deviating from the two predicted shell closures. Obvious prolate predominance has been noticed in large mass ranges with $134 \leq N \leq 168$ and $190 \leq N \leq 236$, while nuclear shapes are oblate only in a short mass range before the neutron number reaching the shell closures. Besides, there are some regions with prolate-to-oblate transition, where shape coexistence may occur. According to the shape evolution described by DRHBc, the rate of deformation, represented by $\frac{\partial|\beta_2|}{\partial N}$ in Eq. (7), evolves from positive to negative as the neutron number exceeds the mid-shell within two shell closures, while remaining zero around the mid-shell. This confirms the crossings of S_{2n} between the DRHBc and RCHB results as shown in Fig. 1(b).

Finally, to examine the role of triaxial degrees of freedom, in Fig. 7, we take the triaxial relativistic Hartree-Bogoliubov theory in continuum (TRHBc) [100] to study the potential energy surfaces (PESs) in the (β, γ) plane for ^{267}Bk and ^{331}Bk , which are predicted to exhibit possible shape coexistence based on the axial DRHBc PECs in Fig. 5. The constrained TRHBc calculations

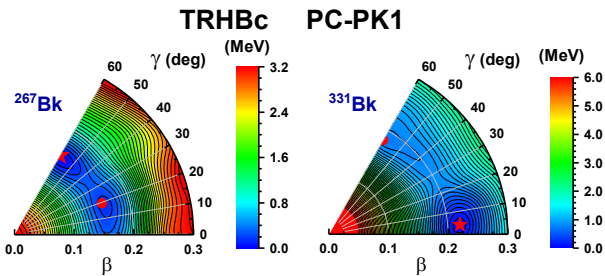


Figure 7: (Color online) Potential energy surfaces (PESs) in the (β, γ) plane for ^{267}Bk and ^{331}Bk calculated by the triaxial relativistic Hartree-Bogoliubov theory in continuum (TRHBc) with PC-PK1. For each nucleus, the global and second local minima are respectively represented by the red stars and dots. The energy separation between the contour lines is 0.1 MeV.

are performed with deformation steps of $\Delta\beta = 0.05$ and $\Delta\gamma = 6^\circ$. Global and local minima are indicated by red stars and dots, respectively. For ^{267}Bk , the TRHBc theory predicts an oblate ground state at $\beta_2 = -0.15$ and a triaxial local minimum at $(\beta = 0.16, \gamma = 19^\circ)$. A clear γ -soft path connects the two minima, separated by a barrier of approximately 0.3 MeV. For ^{331}Bk , the TRHBc calculations yield a nearly prolate ground state at $(\beta = 0.22, \gamma = 4^\circ)$ and an oblate local minimum at $\beta_2 = 0.18$, with a barrier height of approximately 0.9 MeV. These results confirm that the possible shape coexistence predicted in ^{331}Bk by the DRHBc theory persists when triaxiality is taken into account.

IV. SUMMARY

In this work, the ground-state properties and structure evolutions of odd- A transuranium Bk isotopes have been studied by the deformed relativistic Hartree-Bogoliubov theory in continuum, and compared with the available experimental data and the spherical RCHB results. In comparison with RCHB, DRHBc gives a better description for the binding energies E_b , two-neutron separation energies S_{2n} , two-proton separation energies S_{2p} , and α -decay energies Q_α for the Bk isotopes, which align well with the experimental data. Significant deformation effects have been verified in the ground-state properties and structures of the Bk isotopes.

First, with the inclusion of deformation in DRHBc, additional binding energies are contributed. Consequently, remarkable crossings of S_{2n} between RCHB and DRHBc occur within two shell closures, and larger S_{2p} of the DRHBc are found. This further leads to significantly reduced Q_α values before mid-shells by DRHBc. Moreover,

crossings of neutron Fermi energy λ_n between DRHBc and RCHB within two shell closures can also be observed, which can be attributed to the distinct single-particle level structures in the spherical and deformed cases. Meanwhile, the lower proton Fermi energy λ_p of DRHBc is predicted. Based on S_{2n} and S_{2p} along with λ_n and λ_p , the DRHBc theory predicts that the proton and neutron drip lines of the Bk isotopes are ^{227}Bk and ^{355}Bk , respectively.

Second, DRHBc predicts more delicate shell structures. Besides the major shell closures at $N = 184, 258$, which can also be predicted by RCHB, possible sub-shells at $N = 142, 150, 162, 178, 218$, and 230 are identified by the locations of the peaks of the two-neutron gaps δ_{2n} and vanishing neutron pairing energies E_{pair}^n within the framework of DRHBc. Furthermore, distinct kink structures are revealed for S_{2p} and λ_p at the shell closures of $N = 184, 258$.

Finally, according to the evolutions of the ground state deformation β_2 , the nuclear shape undergoes prolate, oblate, and spherical transitions between two shell closures. Obvious prolate dominance has been noted in large mass ranges with $134 \leq N \leq 168$ and $190 \leq N \leq 236$, while nuclear shapes are spherical at shell closures of $N = 184, 258$ and oblate in a short range before reaching the shell closures. Besides, there are some regions with prolate-to-oblate transitions with energy competition between oblate and prolate minima. Possible shape coexistence for ^{267}Bk and ^{331}Bk is predicted by DRHBc, which is supported by the TRHBc calculations for ^{331}Bk but inclined to γ -soft for ^{267}Bk .

Acknowledgments

The authors would like to express their sincere appreciation to Dr. Kai-Yuan Zhang, Dr. Cong Pan, and Prof. Jiang-Ming Yao for their valuable insights and meticulous review of the manuscript. This work was partly supported by the Natural Science Foundation of Henan Province (No. 242300421156), the National Natural Science Foundation of China (No. U2032141, No. 12481540215, and No. 12435006), the Open Project of Guangxi Key Laboratory of Nuclear Physics and Nuclear Technology (No. NLK2022-02), the Central Government Guidance Funds for Local Scientific and Technological Development, China (No. Guike ZY22096024), National Key R&D Program of China (No. 2024YFE0109803), State Key Laboratory of Nuclear Physics and Technology, Peking University (No. NPT2023ZX03), and the Fundamental Research Funds for the Central Universities.

[1] M. Thoennessen, *Transuranium Elements* (Springer, New York, 2016).

[2] K. Morita, K. Morimoto, D. Kaji, et al., J. Phys. Soc.

- Jpn. **73**, 2593 (2004).
- [3] S. Y. Cai, *Man-made elements(in Chinese)* (Shanghai Popular Science Press, Shanghai, 2006).
- [4] W. D. Myers and W. J. Swiatecki, Nucl. Phys. **81**, 1 (1966).
- [5] C. Y. Wong, Phys. Lett. **21**, 688 (1966).
- [6] A. Sobiczewski, F. A. Gareev, and B. N. Kalinkin, Phys. Lett. **22**, 500 (1966).
- [7] V. M. Strutinskii, Yad. Fiz. **3**, 614 (1966).
- [8] H. Meldner, Ark. Fys. A **36**, 593 (1967).
- [9] A. Sobiczewski, Z. Szymański, S. Wycech, et al., Nucl. Phys. A **131**, 67 (1969).
- [10] U. Mosel and W. Greiner, Z. Angew. Phys. **222**, 261 (1969).
- [11] S. G. Zhou, Nucl. Phys. Rev. **34**, 318 (2017).
- [12] F. S. Zhang, Y. H. Zhang, M. H. Zhang, N. Tang, S. H. Chang, J. J. Li, and W. Cheng, J. Beijing Norm. Univ. **58**, 392 (2022).
- [13] J. C. Yang, G. Zeng, G. Q. Xiao, et al., Chin. Sci. Bull. **65**, 8 (2020).
- [14] C. Seife, Science **309**, 78 (2005).
- [15] S. G. Zhou, Physics **43**, 817 (2014).
- [16] L. L. Li, B. N. Lü, N. Wang, K. Wen, C. J. Xia, Z. H. Zhang, J. Zhao, E. G. Zhao, and S. G. Zhou, Nucl. Phys. Rev. **31**, 253 (2014).
- [17] B. N. Lü, J. Zhao, E. G. Zhao, and S. G. Zhou, *Relativistic Density Functional for Nuclear Structure* (World Scientific, 2016), chap. 5 Superheavy nuclei and fission barriers, pp. 171–217.
- [18] X. T. He, J. W. Wu, X. Y. Zhang, and C. W. Shen, Phys. Rev. C **110**, 104301 (2024).
- [19] M. Ismail, S. G. Abd-Elnasser, A. Adel, I. A. M. Abdul-Magead, and H. M. Elsharkawy, Phys. Rev. C **109**, 014606 (2024).
- [20] V. Y. Denisov, Phys. Rev. C **109**, 044618 (2024).
- [21] Z. H. Zhang, K. Wen, X. T. He, J. Y. Zeng, E. G. Zhao, and S. G. Zhou, Nucl. Phys. Rev. **30**, 268 (2013).
- [22] K. Wen, Z. H. Zhang, E. G. Zhao, and S. G. Zhou, Sci. Sin. **42**, 22 (2012).
- [23] S. Ówiok, S. Hofmann, and W. Nazarewicz, Nucl. Phys. A **573**, 356 (1994).
- [24] G. G. Adamian, N. V. Antonenko, S. N. Kuklin, B. N. Lü, L. A. Malov, and S. G. Zhou, Phys. Rev. C **84**, 024324 (2011).
- [25] F. R. Xu, E. G. Zhao, R. Wyss, and P. M. Walker, Phys. Rev. Lett. **92**, 252501 (2004).
- [26] H. L. Liu, F. R. Xu, and P. M. Walker, Phys. Rev. C **86**, 011301 (2012).
- [27] M. Bender, K. Rutz, P.-G. Reinhard, J. A. Maruhn, and W. Greiner, Phys. Rev. C **58**, 2126 (1998).
- [28] J. P. Delaroche, M. Girod, H. Goutte, and J. Libert, Nucl. Phys. A **771**, 103 (2006).
- [29] R. V. Jolos, L. A. Malov, N. Y. Shirikova, and A. V. Sushkov, J. Phys. G **38**, 115103 (2011).
- [30] K. Zhuang, Z. B. Li, and Y. X. Liu, Commun. Theor. Phys. **57**, 271 (2012).
- [31] Y. Sun, G. L. Long, F. Al-Khudair, and J. A. Sheikh, Phys. Rev. C **77**, 044307 (2008).
- [32] Y. S. Chen, Y. Sun, and Z. C. Gao, Phys. Rev. C **77**, 061305 (2008).
- [33] F. Al-Khudair, G. L. Long, and Y. Sun, Phys. Rev. C **79**, 034320 (2009).
- [34] J. W. Cui, X. R. Zhou, F. Q. Chen, Y. Sun, C. L. Wu, and Z. C. Gao, Phys. Rev. C **90**, 014321 (2014).
- [35] J. Egido and P. Ring, J. Phys. G **8**, L43 (1982).
- [36] J. L. Egido and P. Ring, Nucl. Phys. A **423**, 93 (1984).
- [37] X. T. He, Z. Z. Ren, S. X. Liu, and E. G. Zhao, Nucl. Phys. A **817**, 45 (2009).
- [38] Q. H. Mo, M. Liu, and N. Wang, Phys. Rev. C **90**, 024320 (2014).
- [39] K. Rutz, M. Bender, T. Bürvenich, et al., Phys. Rev. C **56**, 238 (1997).
- [40] W. Zhang, J. Meng, S. Zhang, L. Geng, and H. Toki, Nucl. Phys. A **753**, 106 (2005).
- [41] X. R. Zhou and H. Sagawa, J. Phys. G **39**, 085104 (2012).
- [42] J. J. Li, W. H. Long, J. Margueron, and N. van Giai, Phys. Lett. B **732**, 169 (2014).
- [43] Z. Patyk and A. Sobiczewski, Nucl. Phys. A **533**, 132 (1991).
- [44] J. C. Pei, F. R. Xu, Z. Y. Wu, and E. G. Zhao, Nuclear Physics Review **20**, 116 (2003).
- [45] A. Bohr and B. R. Mottelson, *Nuclear Structure* (World Scientific, New York, 1998).
- [46] T. T. Sun, B. X. Li, and K. Liu, Phys. Rev. C **109**, 014323 (2024).
- [47] S. G. Zhou, J. Meng, P. Ring, and E. G. Zhao, Phys. Rev. C **82**, 011301 (2010).
- [48] S. G. Zhou, J. Meng, P. Ring, and E. G. Zhao, J. Phys. **312**, 092067 (2011).
- [49] L. L. Li, J. Meng, P. Ring, E. G. Zhao, and S. G. Zhou, AIP Conference Proceedings **1491**, 208 (2012).
- [50] T. T. Sun, L. Qian, C. Chen, P. Ring, and Z. P. Li, Phys. Rev. C **101**, 014321 (2020).
- [51] Phys. Lett. B **849**, 138422 (2024).
- [52] W. Zhang, J. K. Huang, T.-T. Sun, J. Peng, and S. Q. Zhang, Chin. Phys. C **48**, 104105 (2024).
- [53] P. Möller, A. J. Sierk, T. Ichikawa, et al., Phys. Rev. C **79**, 064304 (2009).
- [54] S. G. Zhou, Phys. Scr. **91**, 063008 (2016).
- [55] K. Heyde and J. L. Wood, Rev. Mod. Phys. **83**, 1467 (2011).
- [56] C. Chen, Q. K. Sun, Y. X. Li, and T. T. Sun, Sci. Chin. **64**, 282011 (2021).
- [57] Q. K. Sun, T. T. Sun, W. Zhang, S. S. Zhang, and C. Chen, Chin. Phys. C **46**, 074106 (2022).
- [58] S. H. Cheng, Z. S. Ge, L. G. Cao, and F. S. Zhang, J. Phys. G **48**, 095106 (2021).
- [59] N. Tsunoda, T. Otsuka, K. Takayanagi, et al., Nature **587**, 66 (2020).
- [60] L. L. Li, J. Meng, P. Ring, E. G. Zhao, and S. G. Zhou, Phys. Rev. C **85**, 024312 (2012).
- [61] K. Y. Zhang, M. K. Cheoun, Y. B. Choi, et al., Phys. Rev. C **102**, 024314 (2020).
- [62] X. X. Sun, J. Zhao, and S. G. Zhou, Nucl. Phys. A **1003**, 122011 (2020).
- [63] X. X. Sun, Phys. Rev. C **103**, 054315 (2021).
- [64] K. Y. Zhang, S. Q. Yang, J. L. An, S. S. Zhang, P. Papakonstantinou, M. H. Mun, Y. Kim, and H. Yan, Phys. Lett. B **844**, 138112 (2023).
- [65] C. Pan, K. Zhang, and S. Zhang, Phys. Lett. B **855**, 138792 (2024).
- [66] X. X. Sun, J. Zhao, and S. G. Zhou, Phys. Lett. B **785**, 530 (2018).
- [67] K. Y. Zhang, D. Y. Wang, and S. Q. Zhang, Phys. Rev. C **100**, 034312 (2019).
- [68] E. J. In, P. Papakonstantinou, Y. Kim, and S. W. Hong,

- Int. J. Mod. Phys. E **30**, 2150009 (2021).
- [69] S. Kim, M. H. Mun, M. K. Cheoun, and E. Ha, Phys. Rev. C **105**, 034340 (2022).
- [70] P. Guo, C. Pan, Y. C. Zhao, X. K. Du, and S. Q. Zhang, Phys. Rev. C **108**, 014319 (2023).
- [71] X. Y. Zhang, Z. M. Niu, W. Sun, and X. W. Xia, Phys. Rev. C **108**, 024310 (2023).
- [72] M. H. Mun, S. Kim, M. K. Cheoun, W. Y. So, S. Choi, and E. Ha, Phys. Lett. B **847**, 138298 (2023).
- [73] K. Y. Zhang, P. Papakonstantinou, M. H. Mun, Y. Kim, H. Yan, and X. X. Sun, Phys. Rev. C **107**, L041303 (2023).
- [74] R. Y. Zheng, X. X. Sun, G. F. Shen, and L. S. Geng, Chin. Phys. C **48**, 014107 (2024).
- [75] K. Y. Zhang, X. T. He, J. Meng, C. Pan, C. W. Shen, C. Wang, and S. Q. Zhang, Phys. Rev. C **104**, 1021301 (2021).
- [76] C. Pan, K. Y. Zhang, P. S. Chong, et al., Phys. Rev. C **104**, 024331 (2021).
- [77] X. T. He, C. Wang, K. Y. Zhang, and C. W. Shen, Chin. Phys. C **45**, 101001 (2021).
- [78] Y. Xiao, S. Z. Xu, R. Y. Zheng, X. X. Sun, L. S. Geng, and S. S. Zhang, Phys. Lett. B **845**, 138160 (2023).
- [79] Phys. Lett. B **856**, 138922 (2024).
- [80] C. Pan, K. Y. Zhang, and S. Q. Zhang, Int. J. Mod. Phys. E **28**, 1950082 (2019).
- [81] K. Y. Zhang, C. Pan, and S. Q. Zhang, Phys. Rev. C **106**, 024302 (2022).
- [82] X. X. Sun and S. G. Zhou, Sci. Bull. **66**, 2072–2078 (2021).
- [83] W. Sun, K. Y. Zhang, C. Pan, X. H. Fan, S. Q. Zhang, and Z. P. Li, Chin. Phys. C **46**, 064103 (2022).
- [84] J. Khuyagbaatar, A. Yakushev, C. E. Düllmann, D. Ackermann, L.-L. Andersson, M. Asai, M. Block, R. A. Boll, H. Brand, D. M. Cox, et al., Phys. Rev. C **102**, 064602 (2020).
- [85] L. L. Li, J. Meng, P. Ring, E. G. Zhao, and S. G. Zhou, Chin. Phys. Lett. **29**, 042101 (2012).
- [86] G. W. C.E. Price, Phys. Rev. C **36**, 354 (1987).
- [87] S. Perez-Martin and L. M. Robledo, Phys. Rev. C **78**, 014304 (2008).
- [88] C. Pan, M. K. Cheoun, Y. B. Choi, et al., Phys. Rev. C **106**, 014316 (2022).
- [89] S. G. Zhou, J. Meng, and P. Ring, Phys. Rev. C **68**, 034323 (2003).
- [90] X. Q. Wang, X. X. Sun, and S. G. Zhou, Chin. Phys. C **46**, 024107 (2022).
- [91] W. Nrtershäuser, D. Tiedemann, M. Žáková, et al., Phys. Rev. Lett. **102**, 062503 (2009).
- [92] K. Y. Zhang, M. K. Cheoun, Y. B. Choi, and et. al (DRHBc Mass Table Collaboration), At. Data Nucl. Data Tables **144**, 101488 (2022).
- [93] At. Data Nucl. Data Tables **158**, 101661 (2024).
- [94] M. Wang, W. J. Huang, F. G. Kondev, G. Audi, and S. Naimi, Chin. Phys. C **45**, 030003 (2021).
- [95] X. W. Xia, Y. Lim, P. W. Zhao, et al., At. Data Nucl. Data Tables **121**, 1 (2018).
- [96] W. Zhang et al. (In preparation).
- [97] Y. X. Zhang, B. R. Liu, K. Y. Zhang, and J. M. Yao, Phys. Rev. C **110**, 024302 (2024).
- [98] R. Casten, *Nuclear structure from a simple perspective*, vol. 23 (Oxford university press, 2000).
- [99] M. Sugawara, Phys. Rev. C **106**, 024301 (2022).
- [100] K. Y. Zhang, S. Q. Zhang, and J. Meng, Phys. Rev. C **108**, L041301 (2023).